*Journal of Institute of Science and Technology, 24*(2), 76-84 (2019)
*ISSN: 2469-9062 (print), 2467-9240 (e)*
Doi: http://doi.org/10.3126/jist.v24i2.27260

***Research Article***

# STUDY OF TWO FAR INFRARED CAVITIES NEARBY ASYMPTOTIC GIANT BRANCH STARS UNDER INFRARED ASTRONOMICAL SATELLITE MAPS

**A. K. Gautam[1*], B. Aryal[2]**

[1]*Bhaktapur Multiple Campus, Bhaktapur, Nepal*
[2]*Central Department of Physics, Tribhuvan University, Kirtipur, Nepal*
[*]*Corresponding author: arjungautamnpj@gmail.com*

(***Received**: September 15, 2019; **Revised**: December 8, 2019; **Accepted**: December 9, 2019)*

## ABSTRACT

Dust colour temperature, dust mass, visual extinction and Planck function with their distributions in the core region of two far infrared cavities (named FIC04+61 and FIC11-54) found within 3° of AGB stars namely AGB0409+6105 and AGB1105-5451 were studied. Dust colour temperature of the core region of the cavities was found to be (19.4 ± 0.93) K to (20.6 ± 0.65) K and (21.4 ± 0.51) K to (22.6 ± 0.23) K, respectively. The product of dust colour temperature and visual extinction was consistent in the order of $10^{-4}$. The contour maps showed that the low-temperature region has greater mass density and suggests that the distribution of dust mass is homogeneous and isotropic. The distribution of Planck function along with the extension (major diameter) and compression (minor diameter) found to be non-uniform distribution means dust particles were oscillating to get dynamical equilibrium. It further suggests that the dust particles in the cavities might not be in the thermal equilibrium possibly due to pressure-driven events of nearby AGB stars. A negative slope in the transition from 25 μm to 60 μm was our finding regarding far infrared spectral distribution in the cavities. It suggests that the number density of dust particles was less than expected in 60 μm regions.

**Keywords**: Interstellar medium, Asymptotic giant branch, Dust, Infrared astronomical satellite, Cavity

## INTRODUCTION

An asymptotic giant branch (AGB) star is generally believed to be in the last evolutionary phases of a low and intermediate mass star ($M \leq 10\ M_{\odot}$). Most of the AGB stars can be identified as long-period variables (LPVs) with significant amplitude pulsation. The strong pulsation produces shock waves which extend the outer layer of an AGB star for better condition of dust formation (Jones *et al.*, 1981). The radiation pressure on newly formed dust grains may drive dusty stellar winds with high mass-loss rates of $10^{-8}$ -$10^{-4}$ $M_{\odot}$/yr (Bowen, 1988). Due to such dusty stellar winds and evolution of the central stars during the AGB phase, the cold and slowly expanding (10-30 km $s^{-1}$) dust envelopes surrounding AGB stars formed. AGB stars are believed to be the primary source of major stellar objects which can significantly affect the integrated spectral energy distributions (SEDs) of star clusters and galaxies (Cassar *et al*., 2013).

AGB stars were considered the primary source of dust in the interstellar medium (ISM) (Seiss & Pumo, 2006). Because low mass stars do not have a strong wind until they reach the AGB phase, the AGB wind interacts directly with the ISM, rather than with the stellar wind remnants from earlier evolutionary stages, as would be the case for more massive stars (Herwig, 2005). The collision between the stellar wind and the ISM results in the formation of a high-density shell of swept-up interstellar gas, which is pushed outwards into the ISM. Generally, asymptotic giant branch (AGB) stars are classified into oxygen-rich (M-type) and carbon-rich (C-type). But in the catalogue provided by Suh and Kwon (2009), AGB stars are classified into four types: O-rich stars (M-type Miras and OH = IR stars), C-rich stars (C-type stars or carbon stars), S stars, and silicate carbon stars. They presented the catalogue of 2193 O-rich stars, 1167 C-rich stars, 287 S stars and 36 silicate carbon stars (Suh & Kwon, 2009).

Using all sky database of IRAS, Wood *et al.* (1994) studied the images of nearby 100 dark molecular clouds at 60 μm and 100 μm wavelengths. They calculated optical depth, visual extinction of dust and hence proposed an empirical formula relating them. Kiss *et al.* (2004), Koenyves *et al*. (2007) investigated 462 far-infrared loops at 60, and 100 μm IRAS map and studied their luminosity distributions. They concluded that these structures might be formed by high pressure events (e.g., AGB wind) in the past. Odenwald and Rickard (1987), Odenwald (1988) recorded fifteen high Galactic latitude clouds in the 100 μm IRAS maps and studied their far-IR properties. Weinberger and Armsdorfer (2004) found a very large (~ 9°) jet-like structures in the far infrared. They concluded that the structure might form because of the interactions of the wind of the AGB stars with ambient matter. Aryal *et al.* (2010) found two giant bipolar dust emission structures centred on PN NGC 1514 at FIR wavelengths.

Dust colour temperature and dust mass of four far infrared loops located within 1° from nearby pulsars presented by Jha *et al.* (2017). They found the dust colour temperature of the core region lies in the range (19.4±1.2) K to (25.3±1.7) K, whereas the range increased to (33±2) K to (47±3) K for the outer region. They measured average

dust mass of each pixel of the four loops which lie in the range $2.96\times10^{26}$ kg to $1822.2\times10^{26}$ kg. The dust colour temperature and dust mass distribution maps showed that the low temperature region has a higher density as expected. Gautam and Aryal (2019) studied four far infrared cavities near the galactic plane and found a similar value of dust colour temperature and dust mass. Still, they proposed that product of visual extinction and dust colour temperature is consistent. They also showed that dust particles oscillate sinusoidally in the core region of the cavity. A similar method for calculation of dust colour temperature, dust mass, visual extinction and Planck function have been used.

**Far Infrared cavities**

Suh and Kwon (2009) presented infrared two-colour diagrams and found 3003 O-rich, 1168 C-rich, 362 S-type and 35 silicate carbon stars in our Galaxy. Present work was performed for systematic search and selected two far infrared cavities for the study based on following selection criteria: (i) the core region of the hole should have minimum flux at 100 μm IRIS maps, (ii) the primary diameter should be > 0.3° (iii) should be located within 3° of C-rich AGB stars, (iv) should lie in the Galactic plane ($-6° < b < 6°$) and (v) there should be no diffuse optical emission to see far infrared cavities around 1168 C-rich AGB stars at 60 and 100 μm IRIS maps using sky view virtual observatory- http://skyview.gsfc.nasa.gov/current/. Here, two cavities have been selected because both lie at the galactic plane so that a similar type of behaviour may be expected; as a result, one different kind of trend could be obtained. The database of two far infrared (FIR) cavities is listed in Table 1. In the present work, dust colour temperature, the distribution of Planck function along with the compression and extension of the cavities and FIR spectral distribution of the cavities have been studied.

**Table 1. The database of two far infrared cavities nearby AGB stars**

| FIC | α(J2000) (deg) | δ(J2000) (deg) | a (deg) | b (deg) | nearby AGB star |
|---|---|---|---|---|---|
| FIC04+61 | 04 h 09 m 00.0 s | 61° 05' 00.0" | 0.6 | 0.2 | AGB0409+6105 |
| FIC11-54 | 11 h 04 m 17.6 s | -54° 29' 05.5" | 1.0 | 0.5 | AGB1105-5451 |

*The first column represents the name (FICHH+DD). The second column and third columns give positions. The next two columns list the major (a) and minor (b) diameters of the cavities. The last column lists the name of nearby AGB star*

## MATERIALS AND METHODS

Two far infrared cavities at the galactic plane around the AGB stars were found under 60 and 100-micron IRAS maps. A method for calculation of dust colour temperature and Planck function of the dusty environment around the carbon-rich Asymptotic Giant Branch stars are briefly described. For it, the method of calculation for the dust colour temperature, dust mass, visual extinction and the Planck function was used as described by Gautam and Aryal (2019).

**Dust colour temperature**

The dust colour temperature of all pixels of selected two FIR cavities was calculated using 60 and 100 μm IRIS flux densities. For this, the method proposed by Wood *et al.* (1994), and later it was improved by Dupac *et al.* (2003), and Schnee *et al.* (2005) was followed. They derived an expression for dust colour temperature $T_d$ as;

$$T_d = \frac{-96}{\ln\{R \times 0.6^{(3+\beta)}\}}, \text{ where , } R = \frac{F(60\mu m)}{F(100\mu m)} \quad (1)$$

Where β is the spectral emissivity index depends on dust grain properties like composition, size, and compactness. For a pure blackbody, β = 0, the amorphous layer-lattice matter has β ~ 1, and the metals and crystalline dielectrics have β ~ 2 which was used in our calculations. Here, F(60 μm) and F(100 μm) are the flux densities in 60 μm and 100 μm respectively and Eq. (1) can be used for calculation of the dust colour temperature.

**Planck function**

The value of Planck function depends on the wavelength (frequency), and hence temperature. Finally, it was used to calculate the dust mass. The Planck function is given by Beichman *et al*. (1988).

$$B(\nu,T) = \frac{2hc}{\lambda^3}\left(\frac{1}{e^{\frac{hc}{\lambda kT}} - 1}\right) \quad (2)$$

Where, h = Planck constant, c = velocity of light, ν = frequency at which the emission was observed, T = the average dust color temperature of the region. It is clear from the expression that the value of Planck function B (ν, T) for longer wavelength was higher than that of the shorter wavelength. Consequently, the range of B (ν, T) for fixed temperature (say ΔT) goes narrower if the wavelength of the images increases.

**Dust mass**

For the calculation of dust mass, the value of flux density ($F_\nu$) at 100 μm maps is needed, and it was used in the expression given by Hildebrand (1983),

$$M_{dust} = \frac{4a\rho}{3Q(\nu)} \cdot \frac{F(\nu)\, D^2}{B(\nu, T)} \quad (3)$$

Where, weighted grain size (a) = 0.1 μm, grain density (ρ) = 3000 kg $m^{-3}$, grain emissivity ($Q_v$) = 0.0010 (for 100 μm) (Young *et al.*, 1993). So the equation (3) reduces to

$$M_{dust} = 0.4\left[\frac{F(\nu)\, D^2}{B(\nu, T)}\right] \quad (4)$$

This equation (4) was used to calculate the dust mass of the cavity.

**Visual Extinction**

For estimation of visual extinction, Wood *et al.* (1994) provided an empirical formula. According to them, visual extinction is

$$A_v(\text{mag}) = 15.078\,[1 - \exp(-\tau_{100}/641.3)] \quad (5)$$

$$\text{Where, } \tau_{100} = \frac{F_\lambda(100\ \mu\text{m})}{B_\lambda(100\ \mu\text{m}, T_d)} \quad (6)$$

Here, $\tau_{100}$ is optical depth at 100 μm wavelength, $F_\lambda$ is flux density, and $B_\lambda$ is Planck function at 100 μm wavelength.

## RESULTS AND DISCUSSION

Here, two far infrared cavities were selected because both lie at the galactic plane (−6° < b < 6°) so that their similar nature (as expected) can be studied. The physical properties of two Far Infrared cavity candidates were described and compared with the previously published works.

**FIC04+61**

Fig. 1(a) shows the cavity FIC04+61 at 100 μm IRIS map where the symbol '+' represents the central position of the cavity and the position of the AGB star (AGB04+61). Figs. 1(b), 1(d) and 1(f) are contour map of flux density, dust colour temperature and dust mass whereas Figs. 1(c) and 1(h) are linear fit between F(100) & F(60) and $A_V$ & $T_d$ respectively . Figs. 1(e) and 1(g) are Gaussian fit of dust colour temperature and dust mass. There were 333 pixels in the region of interest. The values of flux densities at 60 μm and 100 μm were obtained using FITS image of the field and the ALADIN2.5 software. It was plotted 60 μm versus 100 μm flux densities, as shown in Fig. 1(c). The slope of the best fit line has been used to set the errors. The dust colour temperature ($T_d$) of each pixel was calculated using equation (1) and found in the range (19.4±0.9) K to (20.6±0.7) K. Contour map of flux density, dust colour temperature and dust mass are plotted in Figs. 1(b), 1(d) and 1(f) which show distributed within the core region of the cavity. In the dust colour temperature map Fig. 1 (d), minimum temperature region was elongated along the east-west direction, whereas the maximum temperature region was elongated along the north-south direction. From the contour map of dust colour temperature and dust mass, it is found that the distribution of dust mass is homogeneous and isotropic. Fig. 1(d) shows the dust colour temperature distribution in the cavity. This distribution was found to deviate slightly from the Gaussian shown in Figs. 1(e) and 1(g). The linear fit between F(60) and F(100), between $A_V$ and $T_d$, showed a systematic trend with the perfect correlation coefficient. The Gaussian fit of temperature and mass showed Gaussian-like, i.e., symmetric behaviour. It suggests the role of other possible sources (nearby AGB) in the cavity formation.

Figs. 2(a) and 2(b) show the variation of Planck function along with the extension (major diameter passing through flux minima at 100 μm) and compression (minor diameter passing through flux minima at 100 μm) of the cavity. The slopes of fitted lines were found to be minimum, suggesting a marginal fluctuation along the diameters. But these fluctuations are random means dust particles oscillating. It suggests that the particles are not in thermodynamic equilibrium. Similar nature was obtained in case of the square of diameters and temperature, as shown in Figs. 2(c) and 2 (d).

Figs. 2(a) and 2(b) show the variation of Planck function along with the extension (major diameter passing through flux minima at 100 μm) and compression (minor diameter passing through flux minima at 100 μm) of the cavity. The south-west point or north-west point of the diameter was assumed as a reference point, i.e., the left-end point represents the reference point. The correlation coefficient is shown. The error bars represent the standard error (±se) of the deviation. The slopes of fitted lines were found to be minimum, suggesting a marginal fluctuation along the diameters. These fluctuations are random, where it expects a deviation from the local thermodynamic equilibrium. Similar nature was obtained in case of the square of diameters and temperature, which is shown in Figs. 2(c) and 2(d).

There was a uniform distribution of Planck function along major and minor diameters in case of pulsars (Jha *et al.*, 2017). There was a sinusoidal variation of Planck function along both diameters in case of AGB stars (Gautam & Aryal, 2019). But in this case, there was a non-uniform (random) distribution of Planck function along both diameters which was possibly due to strong wind blow of nearby AGB stars. It has happened due to the reason that pulsars emit radiation, but AGB stars blow wind means throw matter.

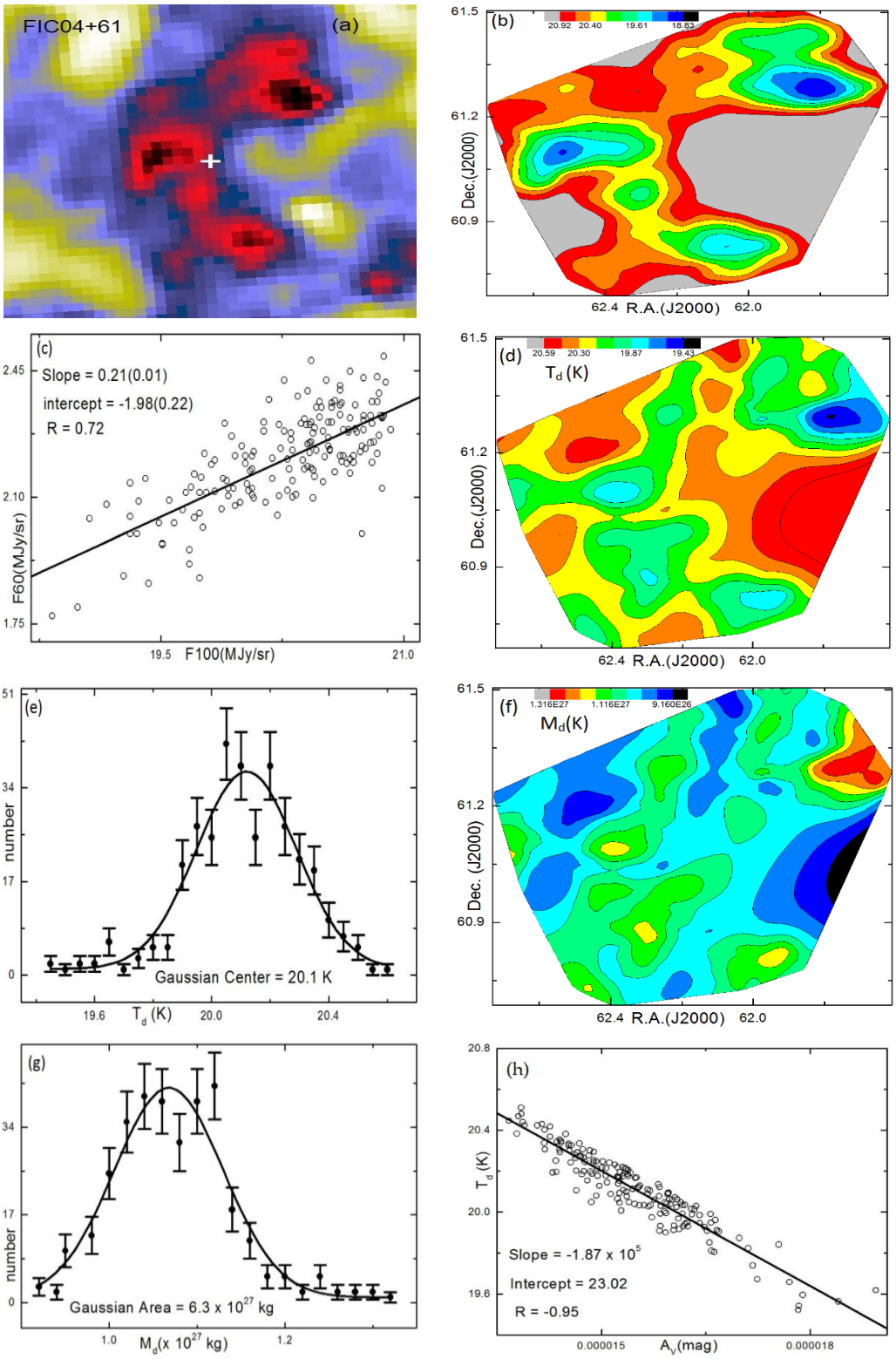


**Fig. 1. IRIS 100 μm JPEG image of the far infrared cavity FIC04+61 centered at R.A. (J2000) = 04h 09m 00s, Dec (J2000) = $61^0$ 05' 00"**

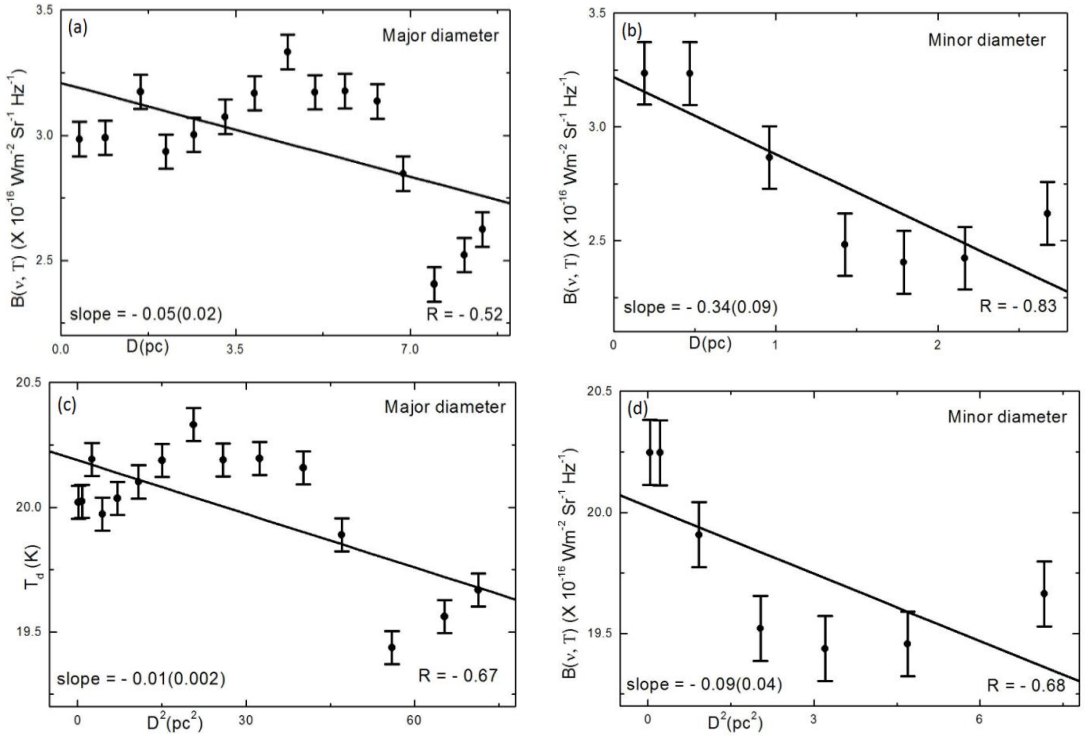


**Fig. 2. Variation of Planck function B(v, T) and dust colour temperature $T_d$(K) of the cavity FIC04+61 with the distance along the major and minor diameter and their squares respectively**

**FIC11-54**

Figure 3(a) shows the cavity FIC11-54 at 100 µm IRIS map. The symbol '+' represents the central position of the cavity and symbol 'x' represents the position of the AGB star (AGB11-54). Figs. 3(b), 3(d) and 3(f) are contour map of flux density, dust colour temperature and dust mass, Figs. 3(c) and 3(h) are a linear fit between F(100) & F(60) and $A_V$ & $T_d$ respectively whereas Figs. 3(e) and 3(g) are Gaussian fit of dust colour temperature and dust mass. There were 782 pixels in the region of interest. The values of flux densities at 60 µm and 100 µm were obtained using FITS image of the field and the ALADIN2.5 software.

Figure 3(c) shows the plot of 60 µm versus 100 µm flux densities and a slope of the best fit line has been used to set the errors. Using equation (1), the dust colour temperature ($T_d$) of each pixel was calculated and found in the range (21.4 ± 0.5) K to (22.6 ± 0.2) K. Contour map of flux density, dust colour temperature and dust mass are plotted in Figs. 3(b), 3(d) and 3(f) which show their distributed within the core region of the cavity. In the dust colour temperature map, as shown in Fig. 3(d), minimum temperature region was elongated along east-west direction whereas the maximum temperature region was elongated along the north-south direction. From the contour map of dust colour temperature and dust mass, it was found that the distribution of dust mass is homogeneous and isotropic. Figure 3(d) shows dust colour temperature distribution in the cavity. This distribution was found to have slightly deviated from the Gaussian shown in Figs. 3(e) and 3(g). The linear fit between F (60) and F(100), between $A_V$ and $T_d$, showed a systematic trend with the excellent correlation coefficient. The Gaussian fit of temperature and mass showed Gaussian-like, i.e., symmetric behaviour. This suggests the role of other possible sources (nearby AGB) in the cavity formation.

Figs. 4(a) and 4(b) show the variation of Planck function along with the extension (major diameter passing through flux minima at 100 µm) and compression (minor diameter passing through flux minima at 100 µm) of the cavity. Figs. 4(c) and 2(d) are the variation of temperature with the square of both diameters, respectively. The south-west point or north-west point of the diameter was assumed as a reference point, i.e., the left-end point represents the reference point. The correlation coefficient is shown. The error bars represent the standard error (±se) of the deviation. The slopes of fitted lines were found to be minimum, suggesting a marginal fluctuation along the diameters. But these fluctuations are random, means dust particles are oscillating. It suggests that the particles were not in thermodynamic equilibrium. Similar nature was obtained in case of the square of diameters and temperature, as shown in Figs. 4(c) and 4(d). It means both cavities showed similar nature in case of distribution of Planck function along both diameters.

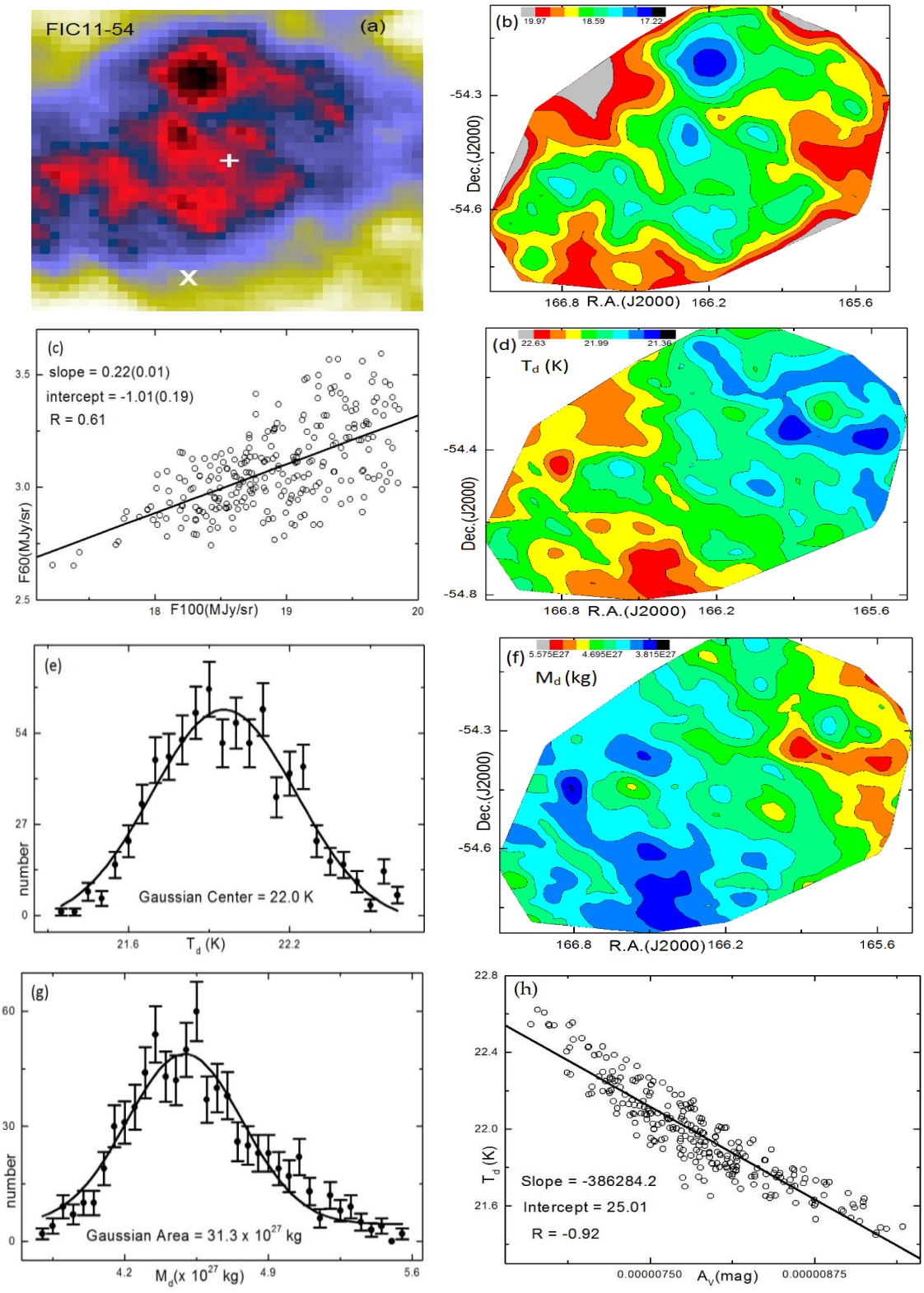


**Fig. 3. IRIS 100 μm JPEG image of the far infrared cavity FIC11-54 centered at R.A. (J2000) = 11h 04m 17.6s, Dec (J2000) = -54$^0$ 29' 05.5"**

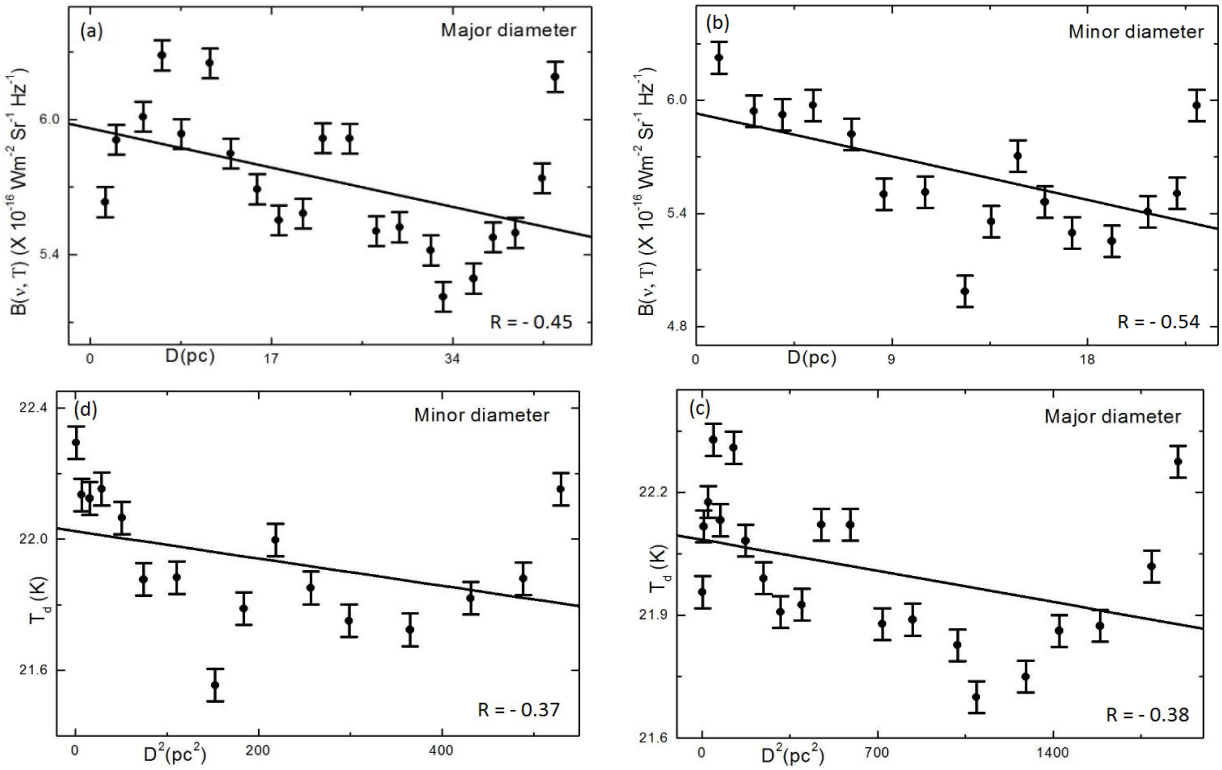


**Fig. 4. Variation of Planck function B(ν, T) and dust colour temperature $T_d$(K) of the cavity FIC04+61 with the distance along the major and minor diameter and their squares respectively**

## DISCUSSION

From the best fit lines between the $T_d$ and $A_V$ of the FIR cavities FIC04+61 and FIC11-54, the relation between them was found to be equation (7) and (8), respectively.

$$T_d = -1.9 \times 10^5 A_V + 23 \quad (7)$$

$$T_d = -3.9 \times 10^5 A_V + 25 \quad (8)$$

After solving them, it was found for FIR cavities FIC04+61 and FIC11-54, respectively, by equations (9) and (10).

$$T_d \times A_V = 1.3 \text{ x } 10^{-4} \quad (9)$$

$$T_d \times A_V = 0.6 \text{ x } 10^{-4} \quad (10)$$

This shows that the product of dust colour temperature and visual extinction of these cavities give nearly similar value. Here, we noticed $T_d \times A_V = \gamma$, where $\gamma$ lies between $0.6 \text{ x } 10^{-4}$ to $1.3 \text{ x } 10^{-4}$, which is comparable with Gautam and Aryal (2019). This value should be calculated for other KK-loops (Koenyves *et al.*, 2007) in the future.

A graph between wavelength and flux density is called spectral distribution. Fig. 5 is an FIR spectral distribution of two cavities where they were compared with Jha *et al.* (2017). Both cavities showed similar nature, i.e., there was a positive slope from 12 µm to 25 µm and 60 µm to 100 µm, but a negative slope from 25 µm to 60 µm. But in the case of infrared cirrus at high latitude molecular cloud, there was a continuous increase in flux density with increase in wavelength Weiland *et al.* (1986). It suggests that fewer dust particles were found in 60 µm wavelength region in case of AGB stars as well as pulsars. It further indicates that there is an interaction between dust and grain at 60 µm wavelength region.

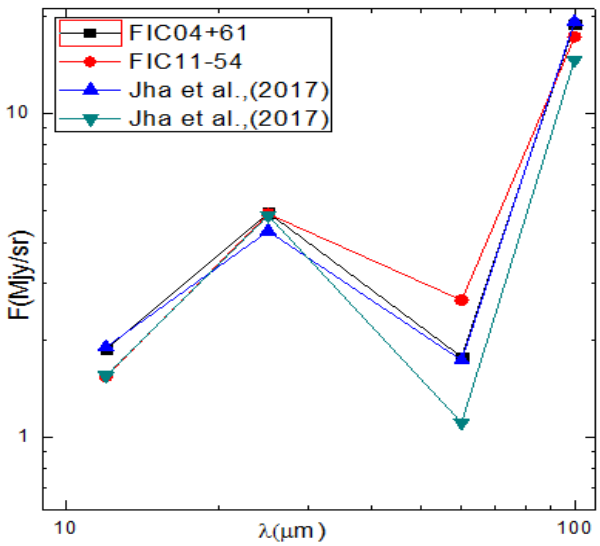


**Fig. 5. FIR spectral distributions of the two cavities compared with the far infrared loops G007+08 and G143+07** (Jha *et al.*, 2017)

## CONCLUSIONS

Physical properties such as dust colour temperature, dust mass, visual extinction and Planck function of two far infrared dusty cavities at 60 µm and 100 µm IRIS maps which were found to be located nearby AGB stars within 3.0° radius has been studied. Conclusions of the results are as follows:

* The values of dust colour temperature lie in the range 19.4 ± 0.93 to 22.6 ± 0.23 K. The dust colour maps showed their distribution where the minimum temperature region was found to be elongated along a north-south direction at the 100 µm flux maxima of all the cavities.
* From the contour map of dust colour temperature and dust mass, distribution of mass was found to be homogeneous and isotropic supporting the cosmological principle.
* In the linear fit between visual extinction and dust colour temperature, a systematic trend with excellent correlation coefficient was noticed, and their product was found similar in the range of $10^{-4}$ which showed that higher the dust colour temperature, lower the visual extinction and vice-versa. It was also verified by their contour maps.
* A fluctuation in the distribution of Planck function along the extension and compression of the FIR cavities was noticed, means dust particles were oscillating in order to get dynamical equilibrium, suggesting the clouds of dust might not be in the thermodynamic equilibrium locally.
* In FIR spectral distribution, a significant decrease in the flux density was noticed from 25 µm to 60 µm in all cavities, which was supported by KK-loops. It means less number density of dust particles were found in 60 µm wavelength region.

## ACKNOWLEDGEMENTS

We acknowledge the Department of Astro-Particle Physics, Innsbrck University, especially to Prof. R. Weinberger for invoking us to work on dusty environments around AGB stars. This research has made use of SkyView Virtual Observatory, Aladin v2.5 and NASA/IPAC Extragalactic Database (NED).

## REFERENCES

Aryal, B., Rajbahak, C., & Weinberger, R. (2010). A giant dusty bipolar structure around the planetary nebula ngc 1514. *Monthly Notices of the Royal Astronomical Society*, *402*, 1307-1312.

Beichman, C. A., Wilson, R. W., Langer, W. D., & Goldsmith, P. F. (1988). Infrared limb brightening in the Barnard 5 cloud. *The Astrophysical Journal Letters*, *332*, L81-L85.

Bowen, G. H. (1988). Dynamical modeling of long-period variable star atmospheres. *The Astrophysical Journal*, *329*, 299-317.

Cassar, L. P., Piovan, L., Weiss, A., Salaris, M., & Chiosi, C. (2013). The role of dust in models of population synthesis. *Monthly Notices of the Royal Astronomical Society*, *436*, 2824-2851.

Dupac, X., Bernard, J. P., Boudet, N., Giard, M., Lamarre, J. M., Meny, C., Pajot, F., Ristorcelli, I., Serra, G., Stepnik, B., & Torre, J. P. (2003). Inverse temperature dependence of the dust submillimeter spectral index. *Astronomy & Astrophysics*, *404*, L11-L15.

Gautam, A. K., & Aryal, B. (2019). A study of four low-latitude (|l| < 10°) far-infrared cavities. *Journal of Astrophysics and Astronomy*, *40*(16), 1-10.

Habing, H. J. (1996). Circumstellar envelopes and asymptotic giant branch stars. *Astronomy and Astrophysics Reviews*, *7*, 97-207.

Herwig, F. (2005). Evolution of asymptotic giant branch stars. *Annual Review of Astronomy and Astrophysics*, *43*, 435-479.

Hildebrand, R. H. (1983). The determination of cloud mass and dust characteristics from sub-millimetre thermal emission. *Royal Astronomical Society*, *24*, 267-282.

Jha, A. K., Aryal, B., & Weinberger, R.. (2017). A study of dust colour temperature and dust mass distributions of four far infrared loops. *Revista Mexicana de Astronomia y Astrofisica*, *53*, 467-476.

Jones, T. W., Ney, E. P., & Stein, W. A. (1981). Pulsations, grain condensation, and mass loss in long-period variable stars. *The Astrophysical Journal*, *250*, 324-326.

Kiss, C., Moór, A., & Tóth, L.V. (2004). Far-infrared loops in the 2nd galactic quadrant. *Astronomy and Astrophysics*, *418*, 131-141.

Koenyves, V., Kiss, Cs., Moor, A., Kiss, Z.T., & Toth, L.V. (2007). Catalogue of far- infrared loops in the galaxy. *Astronomy & Astrophysics*, *463*, 1227-1234.

Odenwald, S. F. (1988). Comet-like clouds at far-infrared and optical wavelengths-mach cones and hydrodynamics. *Astrophysical Journal*, *325***,** 320-341.

Odenwald, S. F., & Rickard, L. J. (1987). Hydrodynamical processes in the Draco molecular cloud. *The Astrophysical Journal*, *318*, 702-711.

Schnee, S. L., Ridge, N. A., Goodman, A. A. & Jason, G. L. (2005). A complete look at the use of IRAS emission maps to estimate extinction and dust temperature. *The Astrophysical Journal*, *634*, 442-450.

Seiss, L., & Pumo, M. L. (2006). Evolutionary properties of massive AGB stars. *Memorie della Societa Astronomica Italiana*, *77*, 822-827.

Suh, K. W. & Kwon, Y. J. (2009). A catalogue of AGB stars in IRAS PSC. *Journal of the Korean Astronomical Society*, *42*, 81-91.

Weiland, J. L., Blitz, L., Dwek, E., Hauser, M. G., Magnani, L., & Rickard, L. J. (1986). Infrared cirrus and high-latitude molecular clouds. *The Astrophysical Journal Letters*, *306*, L101-L104.

Weinberger, R., & Armsdorfer, B. (2004). A pair of gigantic bipolar dust jets close to the solar system. *Astronomy & Astrophysics*, *416*, L27-L30.

Wood, D. O. S., Myers, P. C., & Daugherty, D. A. (1994). IRAS images of nearby dark clouds. *The Astrophysical Journal Supplement*, *95*, 457-501.

Young, K., Phillips, T. G., & Knapp, G. R. (1993). Circumstellar shells resolved in IRAS survey data II analysis. *Astrophysical Journal*, *409*, 725-738.